

Supplementary Materials for
Dual Iron Sites in Activation of N₂ by Iron-Sulfur Cluster Anions Fe₅S₂[−] and
Fe₅S₃[−]

Gui-Duo Jiang,^{†,‡,§} Zi-Yu Li,^{†,§*} Li-Hui Mou,^{†,‡,§} Sheng-Gui He^{†,‡,§*}

[†]State Key Laboratory for Structural Chemistry of Unstable and Stable Species, Institute of Chemistry, Chinese Academy of Sciences, Beijing, 100190, P. R. China

[‡]University of Chinese Academy of Sciences, Beijing, 100049, P. R. China

[§]Beijing National Laboratory for Molecular Sciences and CAS Research/Education Center of Excellence in Molecular Sciences, Beijing, 100190, P. R. China

Content:

- 1. Methods.** (Page S2)
- 2. Additional experimental results.** (Pages S3–S5)
- 3. Additional theoretical results.** (Pages S6–S13)
- 4. References** (Page S14)

1. Methods.

1.1 Experimental Methods.

Details of the experimental setup can be found in our previous studies,^{1,2} and only a brief outline of the experiments is given below. In experiments, a series of iron-sulfur cluster anions were generated by laser ablation of a rotating and translating Fe/S mixed-powder disk target (molar ratio of Fe/S is 10:1) in the presence of a He carrier gas with a backing pressure of about 4 atm. The anion clusters of interest were mass-selected by a quadrupole mass filter (QMF)¹ and then entered into a linear ion trap (LIT)² reactor, in which they were confined and thermalized by collisions with a pulse of He gas for about 1 ms. The thermalized cluster anions subsequently reacted with a pulse of N₂ for about 14.6 ms. The pressures of N₂ were in the range of 1.0–1.5 Pa. The reactant and product ions ejected from the LIT were transferred into a reflectron time-of-flight (TOF) mass spectrometer for mass and intensity measurements.¹

1.2 Theoretical Methods.

Density functional theory (DFT) calculations using Gaussian 09 program³ were carried out to investigate the structures of Fe₅S₁₋₄⁻ as well as the corresponding N₂ adsorption products. A Fortran code⁴ based on a genetic algorithm was used to generate initial guess structures of the clusters. The detailed procedure to perform the genetic algorithm can be found in our previous work. Combined with 6-311+G* basis set⁵, the BPW91 functional⁶ was employed in this work, which has been shown to have good performance for iron-sulfur clusters.⁷ Each initial structure was optimized at various possible spin multiplicities and all relative energies were zero-point energy corrected. The reaction mechanism calculations of Fe₅S₁₋₄⁻ with N₂ by the DFT method involved geometry optimization of reaction intermediates (IMs). Vibrational frequency calculations were further performed to confirm the IMs, which have zero imaginary frequency. Natural bond orbital (NBO) analysis was performed with NBO 6.0⁸ and the program Multiwfn⁹ was employed to perform the projected electronic densities of states (pDOS) and localized molecular orbital (LMO) analysis.

2. Additional experimental results.

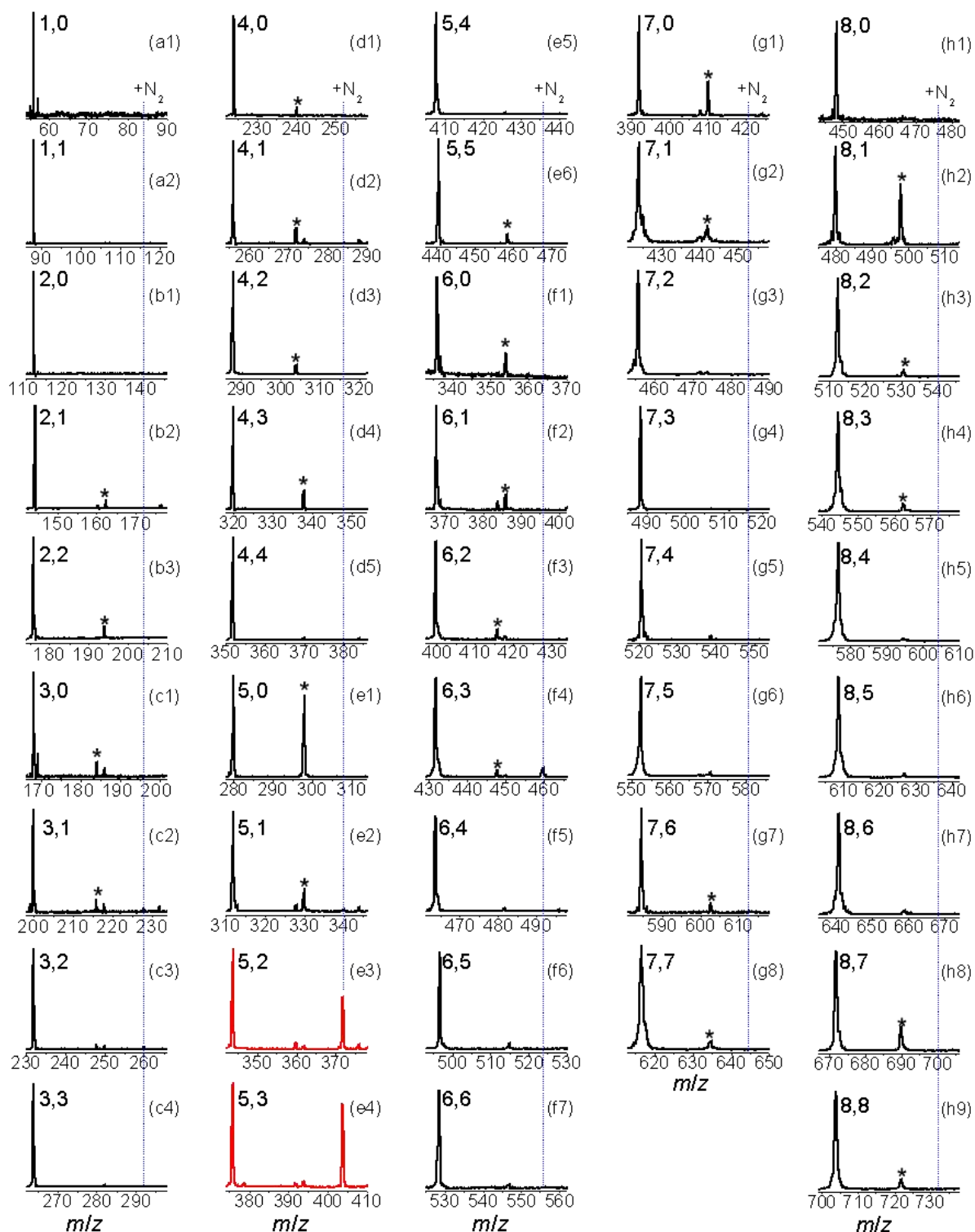


Figure S1. Time-of-flight mass spectra for the reactions of mass-selected Fe_xS_y^- ($x = 1-8$, $y = 0-x$) with 1.0–1.5 Pa N_2 for about 14.6 ms. The Fe_xS_y^- species are denoted as x,y . Peaks marked with asterisks are due to the residual water in the gas handling system. The blue imaginary lines indicate the peaks of N_2 adsorption products.

Table S1. Estimated rate constants (k_1 , 10^{-14} cm³ molecule⁻¹ s⁻¹) for thermal reactions of Fe_xS_y⁻ ($x = 1-8$, $y = 0-x$) clusters with N₂.

Fe _x S _y ⁻	k_1	Fe _x S _y ⁻	k_1	Fe _x S _y ⁻	k_1	Fe _x S _y ⁻	k_1
1,0	≤ 1.4	2,0	≤ 0.5	3,0	≤ 1.4	4,0	≤ 0.9
1,1	≤ 0.3	2,1	≤ 0.7	3,1	2.0	4,1	1.6
—	—	2,2	≤ 0.2	3,2	1.3	4,2	1.1
—	—	—	—	3,3	≤ 0.02	4,3	≤ 0.1
—	—	—	—	—	—	4,4	≤ 0.01
Fe _x S _y ⁻	k_1	Fe _x S _y ⁻	k_1	Fe _x S _y ⁻	k_1	Fe _x S _y ⁻	k_1
5,0	≤ 0.5	6,0	≤ 1.8	7,0	2.2	8,0	≤ 1.6
5,1	1.5	6,1	≤ 0.7	7,1	≤ 1.5	8,1	≤ 0.6
5,2	8.4	6,2	≤ 0.1	7,2	≤ 0.2	8,2	≤ 0.2
5,3	12.0	6,3	4.1	7,3	≤ 0.2	8,3	≤ 0.3
5,4	≤ 0.05	6,4	≤ 0.4	7,4	≤ 0.2	8,4	≤ 0.4
5,5	≤ 0.8	6,5	≤ 0.5	7,5	≤ 0.6	8,5	≤ 0.2
—	—	6,6	≤ 0.3	7,6	≤ 0.6	8,6	≤ 0.3
—	—	—	—	7,7	≤ 0.4	8,7	≤ 0.2
—	—	—	—	—	—	8,8	≤ 0.3

The pseudo-first-order rate constants (k_1) for the reactions of Fe_xS_y⁻ with N₂ were determined by Eq. (1), in which I_R is the intensity of the reactant cluster ions after the reaction, I_T is the total ion intensity including product ion contribution, P is the effective pressure of the reactant gas, k_B is the Boltzmann constant, T is the temperature (298 K) of the reactant gas, and t_R is the reaction time (14.6 ms).

$$\ln \frac{I_R}{I_T} = -k_1 \frac{P}{k_B T} \times t_R \quad (1)$$

When estimating the k_1 value in Eq. (1), the systematic deviations of t_R ($\pm 3\%$), T ($\pm 1\%$), and P ($\pm 20\%$) were considered. For unreactive clusters, the upper limits of the reaction rate constants were estimated. Rate constants k_1 values for the reactions of all investigated Fe_xS_y⁻ with N₂ are presented in Table S1.

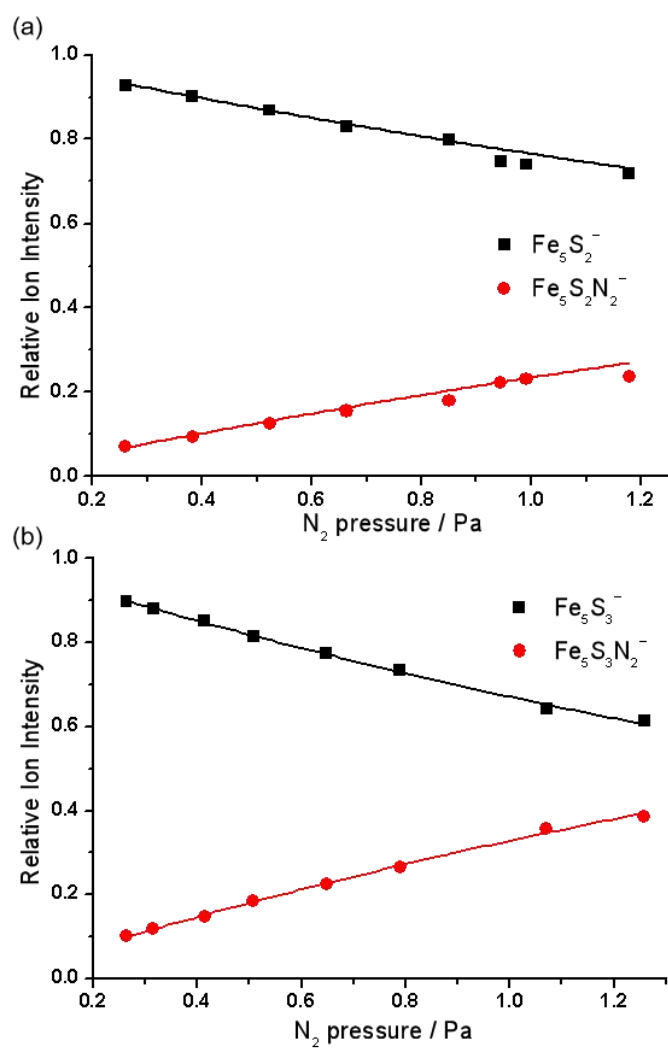


Figure S2. Variations of the relative intensities with respect to the N_2 pressures in the reactions of (a) $Fe_5S_2^-$ and (b) $Fe_5S_3^-$ with N_2 . The data points were experimentally measured, and the solid lines were calculated on the basis of rate constants determined from least-squares fitting.

3. Additional theoretical results.

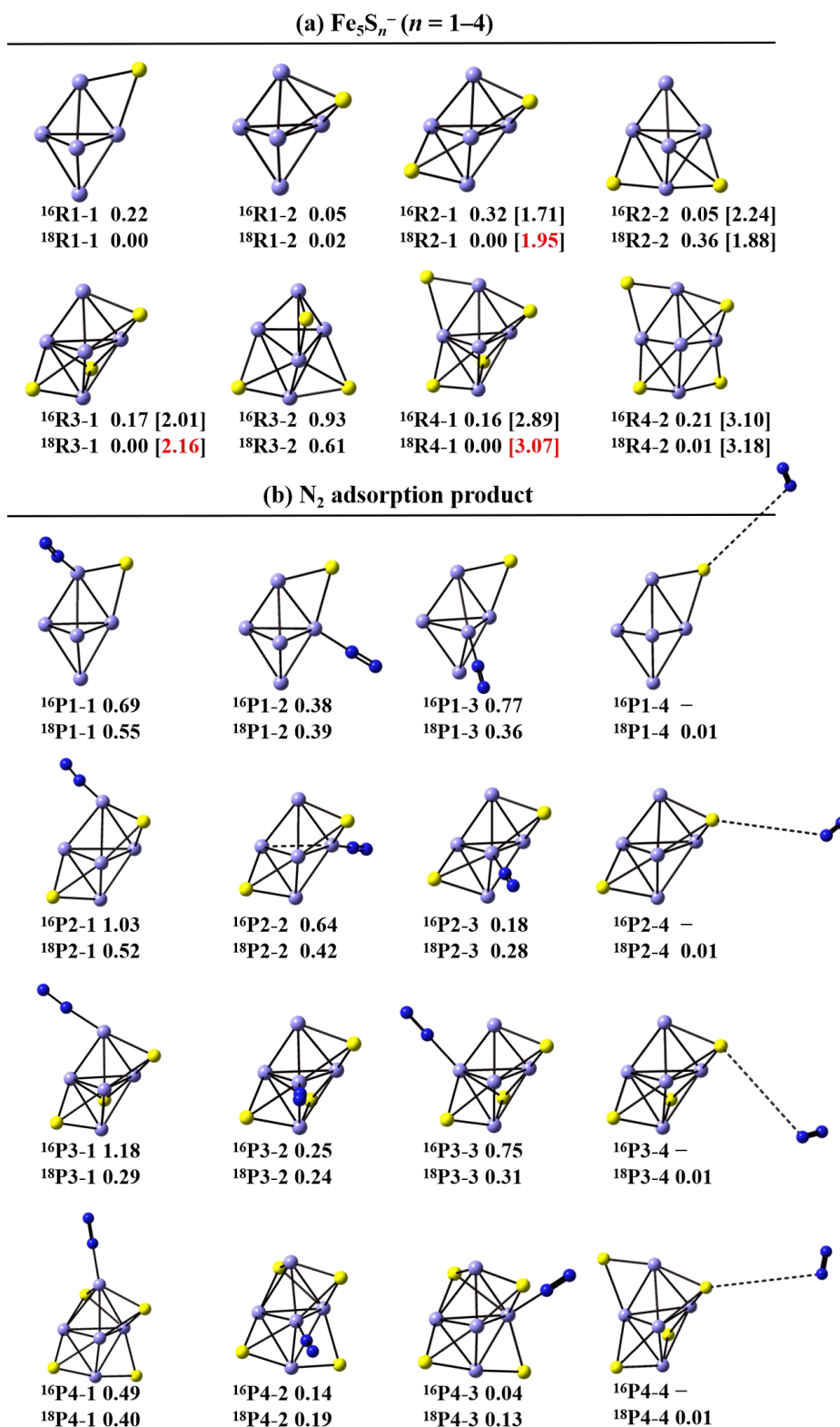


Figure S3. (a) DFT calculated low-lying isomers of Fe_5S_n^- ($n = 1-4$). The relative energies (ΔH , in eV) of Fe_5S_n^- ($Rn-i$) with respect to the lowest-lying isomer ($Rn-1$) are given. The DFT calculated vertical detachment energy (VDE) values are shown in the square brackets. (b) DFT calculated low-lying isomers of $\text{Fe}_5\text{S}_n\text{N}_2^-$ ($n = 1-4$). The adsorption energies of $\text{Fe}_5\text{S}_n\text{N}_2^-$ ($Pn-i$) with respect to the separated reactants (Fe_5S_n^- and N_2) in eV are listed. The superscripts indicate spin multiplicities.

The lowest lying isomer of Fe_5S^- is predicted to have a Fe_5 trigonal bipyramid skeleton and a 2-fold coordinated S atom with a spin multiplicity of 18 ($^{18}\text{R1-1}$). A low lying isomer with a 3-fold coordinated S atom ($^{18}\text{R1-2}$) is 0.02 eV higher than $^{18}\text{R1-1}$ in energy. Both isomers with a spin multiplicity of 16 ($^{16}\text{R1-1}$ and $^{16}\text{R1-2}$) lie slightly higher (< 0.3 eV) in energy than those with a spin multiplicity of 18 ($^{18}\text{R1-1}$ and $^{18}\text{R1-2}$). Thus, all four isomers are possible candidates of Fe_5S^- generated in experiments. Furthermore, the conversion of $^{18}\text{R1-2}$ to $^{18}\text{R1-1}$ is feasible with a small energy barrier of 0.20 eV with respect to the lowest lying isomer ($^{18}\text{R1-1}$).

The lowest lying isomer of Fe_5S_2^- is predicted to have a Fe_5 skeleton capped by two sulfur atoms on the opposite 3-fold hollow sites ($^{18}\text{R2-1}$). A low lying isomer with a spin multiplicity of 16 with one 2-fold S atom and one 3-fold S atom ($^{16}\text{R2-2}$) is only 0.05 eV higher than $^{18}\text{R2-1}$ in energy. While $^{18}\text{R2-1}$ is the most possible species of Fe_5S_2^- generated in experiments due to the well match of calculated vertical detachment energy (VDE) with the experimental value (1.95 eV vs 1.97 eV) and $^{16}\text{R2-2}$ may be excluded due to the mismatch of the calculated VDE value with the experimental value (2.24 eV vs 1.97 eV).

The lowest lying isomer of Fe_5S_3^- is predicted to have three 3-fold coordinated S atoms in the Fe_5 trigonal bipyramid skeleton ($^{18}\text{R3-1}$). The isomer with a spin multiplicity of 16 ($^{16}\text{R3-1}$) is 0.17 eV higher in energy than that with a spin multiplicity of 18 ($^{18}\text{R3-1}$). While $^{18}\text{R3-1}$ is the most possible species of Fe_5S_3^- generated in experiments due to the reasonable match of the calculated VDE value with the experimental value (2.16 eV vs 2.41 eV) and $^{16}\text{R3-1}$ may be ruled out due to the mismatch of the calculated VDE value with the experimental value (2.01 eV vs 2.41 eV).

The lowest lying isomer of Fe_5S_4^- is predicted to have three 3-fold coordinated S atoms and one 2-fold coordinated S atom in the Fe_5 trigonal bipyramid skeleton ($^{18}\text{R4-1}$). A low lying isomer with two 3-fold coordinated S atoms and two 2-fold coordinated S atoms ($^{18}\text{R4-2}$) is only 0.01 eV higher in energy than $^{18}\text{R4-1}$. The isomers with a spin multiplicity of 16 ($^{16}\text{R4-1}$ and $^{16}\text{R4-2}$) are 0.16 eV and 0.20 eV higher in energy than those with a spin multiplicity of 18 ($^{18}\text{R4-1}$ and $^{18}\text{R4-2}$). Thus, all four isomers are possible candidates of Fe_5S_4^- generated in experiments. Note that the transformation from $^{18}\text{R4-2}$ to $^{18}\text{R4-1}$ has a negligible energy barrier of 0.02 eV.

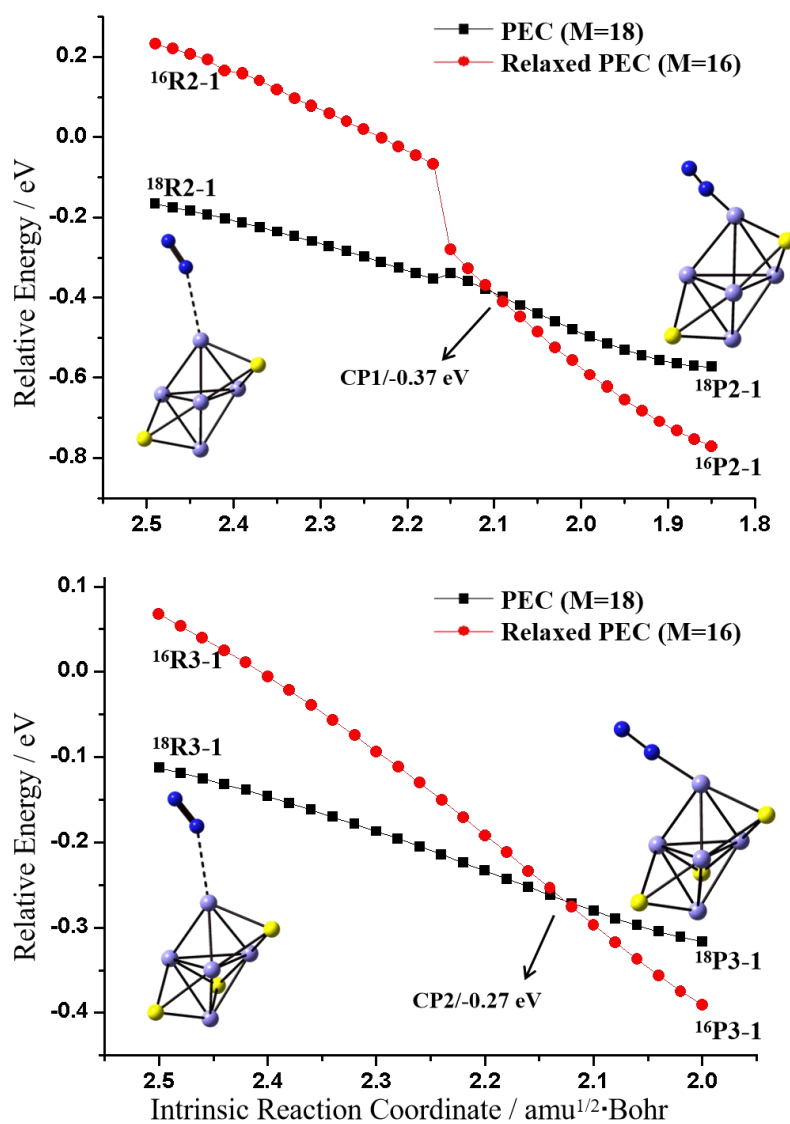


Figure S4. DFT-calculated potential-energy curves (PECs) for spin conversions occurring in the reactions of $\text{Fe}_5\text{S}_{2,3}^-$ with N_2 ($^{18}\text{R2} + \text{N}_2 \rightarrow ^{16}\text{P2}$ and $^{18}\text{R3} + \text{N}_2 \rightarrow ^{16}\text{P3}$) in the main text. The relative energies (ΔH , in eV) are with respect to the separate reactants ($^{18}\text{R2}/^{18}\text{R3}$ and N_2). M values indicate spin multiplicities.

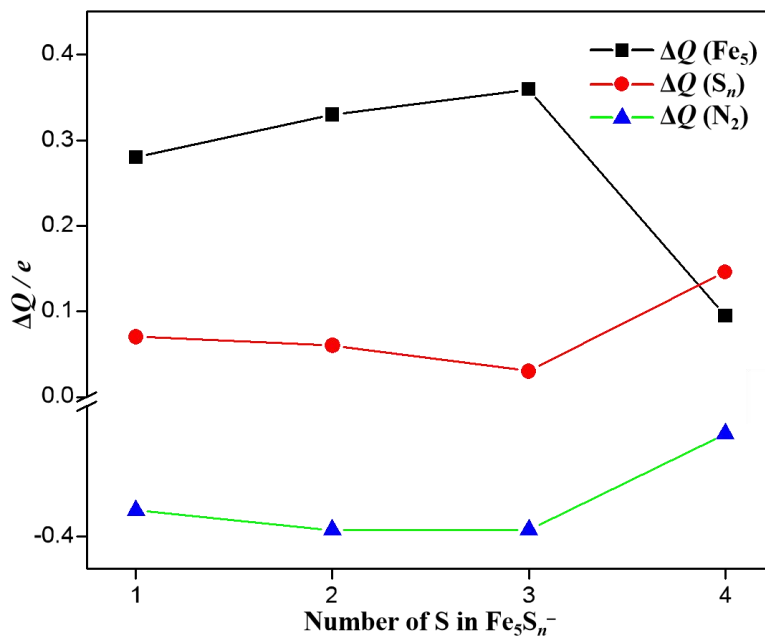


Figure S5. The natural charge difference (ΔQ) of Fe_5 unit, S_n unit and N_2 unit upon the process of N_2 adsorption toward $\text{Fe}_5\text{S}_{1-4}^-$.

As shown in Figure S5, Fe_5 units in $\text{Fe}_5\text{S}_{1-3}^-$ are regarded as main electron donors to trap N_2 and the electron donating ability of the metal centers (Fe_5) strengthens from Fe_5S^- to Fe_5S_3^- and dramatically weakens in $\text{Fe}_5\text{S}_4^-/\text{N}_2$ system. In $\text{Fe}_5\text{S}_4^-/\text{N}_2$ system, both metal centers and sulfur ligands act as electron donors in the adsorption and activation of N_2 . It is noteworthy that the N_2 unit in $\text{Fe}_5\text{S}_4^-/\text{N}_2$ reaction system is least activated as reflected by the less electrons gained from Fe_5S_4^- compared to other systems.

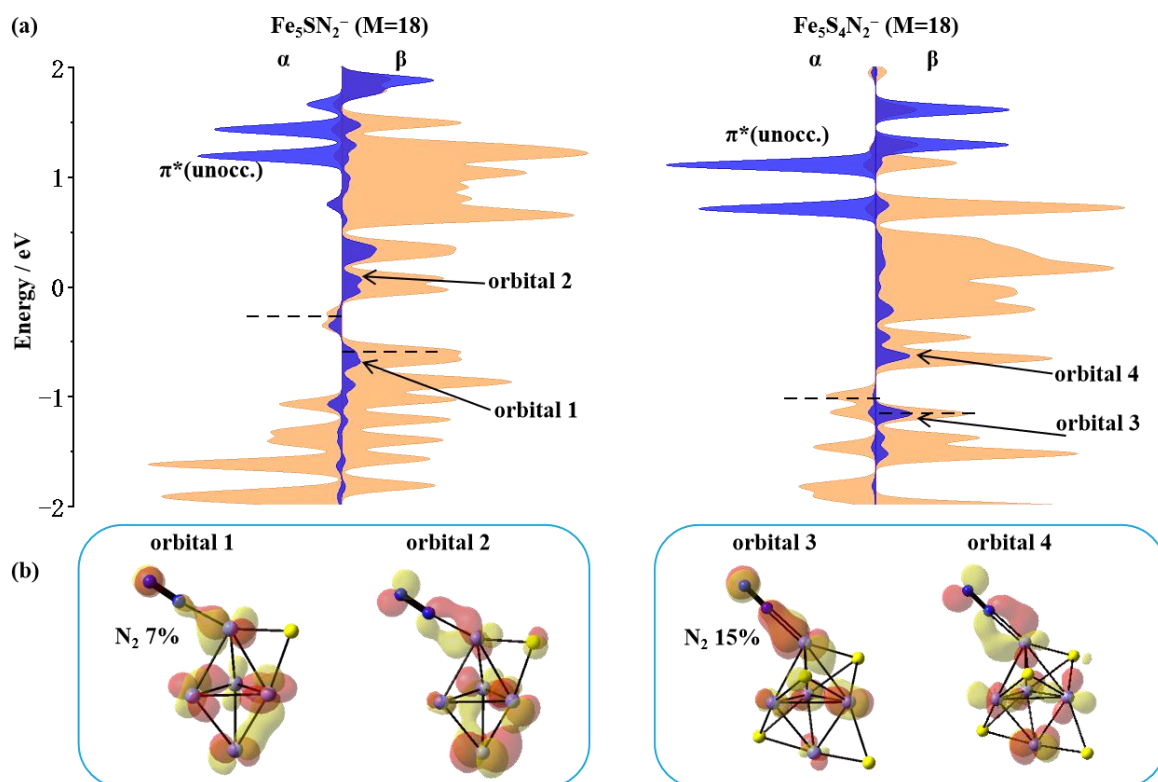


Figure S6. (a) Projected electronic densities of states (pDOS) and schematic illustrations of 3d orbitals of Fe_5 unit and 2p-orbitals of N_2 molecule in $\text{Fe}_5\text{S}_{1.4}\text{N}_2^-$ (M=18, M indicates the spin multiplicity). Orange fillings stand for 3d orbitals of Fe_5 unit and blue fillings stand for 2p-orbitals of N_2 . The black dashed lines indicate the positions of the HOMO. All energies are shown relative to the Fermi level. (b) The profiles of four interesting β orbitals (orbitals 1–4) marked in (a). The percentages of the localized molecular orbitals (LMOs) on N_2 unit are listed.

Different from the unexpected back-donation interactions involving $d-d$ bonding orbitals of dual iron sites in $\text{Fe}_5\text{S}_{2.3}\text{N}_2^-$, classical back-donation interactions between symmetry matched d orbitals (d_{xz} or d_{yz}) of the adsorption site and π^* orbitals of N_2 in $\text{Fe}_5\text{S}_{1.4}\text{N}_2^-$ are drawn clearly in Figure S6. It is noteworthy that only one π^* orbital (π_x^*) is partially occupied while the other π^* orbital (π_y^*) is totally unoccupied in $\text{Fe}_5\text{S}_{1.4}\text{N}_2^-$, which may lead to less overlap and smaller population of electron densities on N_2 unit than the unexpected back-donation interactions resulting in more overlap between $d-d$ bonding orbitals and two π^* (π_x^* and π_y^*) orbitals.

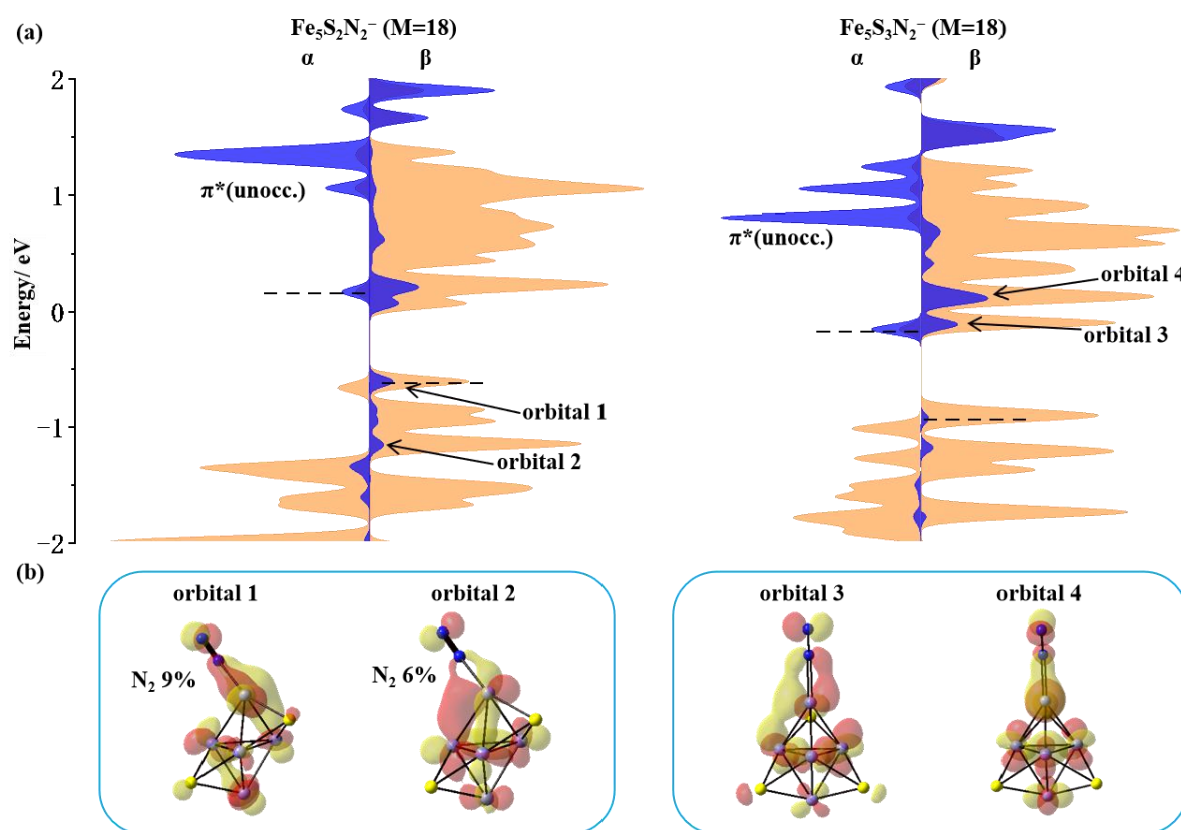
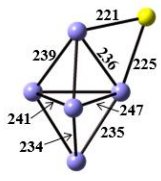
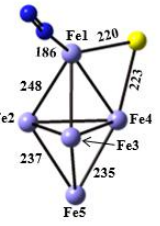
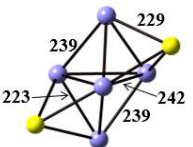
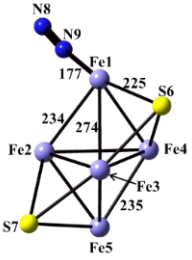
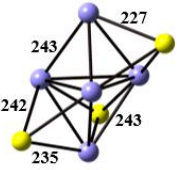
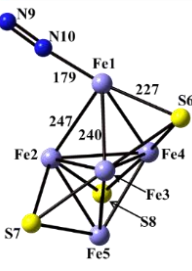
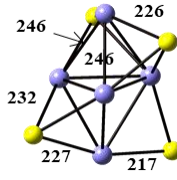
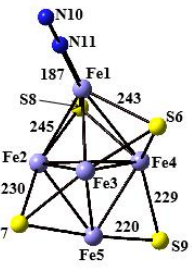


Figure S7. (a) Projected electronic densities of states (pDOS) and schematic illustrations of $3d$ orbitals of Fe_5 unit and $2p$ -orbitals of N_2 molecule in $\text{Fe}_5\text{S}_{2.3}\text{N}_2^-$ ($M=18$, M indicates the spin multiplicity). Orange fillings stand for $3d$ orbitals of Fe_5 unit and blue fillings stand for $2p$ -orbitals of N_2 . The black dashed lines indicate the positions of the HOMO. All energies are shown relative to the Fermi level. (b) The profiles of four interesting β orbitals (orbitals 1–4) marked in (a). The percentages of the localized molecular orbitals (LMOs) on N_2 unit are listed.

As shown in Figure S3, isomers of $\text{Fe}_5\text{S}_{1-4}^-$ with a spin multiplicity of 18 can only weakly bind N_2 with the binding energy in a range of 0.29~0.55 eV, while the isomers with a spin multiplicity of 16 can bind N_2 with larger adsorption energies. Therefore, it can be concluded that the isomers with a spin multiplicity of 16 (^{16}R) may have higher reactivity towards N_2 than those with a spin multiplicity of 18 (^{18}R). In order to understand how the spin state controls the reactivity of the iron-sulfur cluster, the N_2 adsorption process toward $\text{Fe}_5\text{S}_{2.3}^-$ with a spin multiplicity of 18 was analyzed. There are more electron occupancy in the valence $4s$ orbital of $\text{Fe}_5\text{S}_{2.3}^-$ with a spin multiplicity of 18 ($4s^{0.79}$ and $4s^{0.64}$, respectively) than that of $\text{Fe}_5\text{S}_{2.3}^-$ with a spin multiplicity of 16 ($4s^{0.71}$ and $4s^{0.55}$, respectively), which leads to more σ repulsion and is responsible for the small binding energy of $^{18}\text{Fe}_5\text{S}_{2.3}^-$. Besides, as shown in Figure S7, the orbital interactions between metal centers and N_2 in $^{18}\text{Fe}_5\text{S}_2\text{N}_2^-$ are weak, with inefficient orbital overlap and less characters of nitrogen π^* orbitals. As for $^{18}\text{Fe}_5\text{S}_3\text{N}_2^-$, the two back-donation orbitals are unoccupied due to the high energy levels.

Table S2. The spin densities and electron occupancy on each atom and bond lengths (pm) of Fe–N, Fe–Fe, and Fe–S in Fe_5S_n^- and $\text{Fe}_5\text{S}_n\text{N}_2^-$ ($n = 1-4$). $\Delta(e)$ is the electron occupancy change of each atom in $\text{Fe}_5\text{S}_{1-4}^-$ compared with the corresponding isolated atom.

		Atom	Spin densities (ρ)			Electron occupancy	
			Rn	Pn	$\Delta\rho$	Rn	Δe
		Fe1	3.12	2.56	-0.56	$4s^{0.72}3d^{6.92}$	0.36
		Fe2	3.58	3.70	0.13	$4s^{1.22}3d^{6.88}$	-0.10
		Fe3	3.58	3.71	0.13	$4s^{1.22}3d^{6.88}$	-0.10
		Fe4	3.04	3.10	0.07	$4s^{0.69}3d^{6.93}$	0.38
		Fe5	3.30	3.51	0.21	$4s^{1.24}3d^{6.87}$	-0.11
		S6	0.39	0.37	-0.02	$3s^{1.89}3p^{5.02}$	-0.91
		N7	0.00	0.00	0.00	-	-
		N8	0.00	0.04	0.04	-	-
		Fe1	3.04	1.98	-1.05	$4s^{0.76}3d^{6.95}$	0.29
		Fe2	2.85	3.01	0.17	$4s^{0.74}3d^{7.05}$	0.21
		Fe3	2.83	2.86	0.03	$4s^{0.55}3d^{7.07}$	0.38
		Fe4	2.84	3.38	0.54	$4s^{0.74}3d^{7.05}$	0.21
		Fe5	3.04	3.33	0.29	$4s^{0.76}3d^{6.95}$	0.29
		S6	0.20	0.26	0.06	$3s^{1.87}3p^{5.01}$	-0.88
		S7	0.20	0.31	0.10	$3s^{1.87}3p^{5.01}$	-0.88
		N8	0.00	-0.11	-0.11	-	-
		N9	0.00	-0.02	-0.02	-	-
		Fe1	2.91	2.40	-0.52	$4s^{0.62}3d^{6.99}$	0.39
		Fe2	2.86	3.02	0.16	$4s^{0.56}3d^{7.09}$	0.35
		Fe3	2.73	2.87	0.14	$4s^{0.48}3d^{6.91}$	0.61
		Fe4	2.73	2.87	0.14	$4s^{0.52}3d^{7.02}$	0.46
		Fe5	3.04	3.09	0.05	$4s^{0.56}3d^{7.09}$	0.35
		S6	0.23	0.20	-0.03	$3s^{1.87}3p^{4.99}$	-0.86
		S7	0.25	0.33	0.08	$3s^{1.87}3p^{4.99}$	-0.86
		S8	0.25	0.33	0.09	$3s^{1.85}3p^{4.95}$	-0.80
		N9	0.00	-0.12	-0.12	-	-
		N10	0.00	0.00	0.00	-	-
		Fe1	3.11	2.68	-0.43	$4s^{0.50}3d^{6.87}$	0.63
		Fe2	3.00	3.00	0.00	$4s^{0.54}3d^{6.93}$	0.53
		Fe3	3.00	3.02	0.02	$4s^{0.54}3d^{6.93}$	0.53
		Fe4	3.09	3.17	0.08	$4s^{0.46}3d^{6.86}$	0.68
		Fe5	3.08	3.16	0.07	$4s^{0.54}3d^{6.86}$	0.60
		S6	0.42	0.57	0.16	$3s^{1.87}3p^{4.93}$	-0.80
		S7	0.32	0.29	-0.03	$3s^{1.88}3p^{4.92}$	-0.80
		S8	-0.84	-0.79	0.05	$3s^{1.85}3p^{4.95}$	-0.80
		S9	-0.83	-0.80	0.03	$3s^{1.87}3p^{4.93}$	-0.80
		N10	0.00	0.03	0.03	-	-
		N11	0.00	0.01	0.01	-	-

Spin density differences ($\Delta\rho$) upon the process of N_2 adsorption toward $Fe_5S_{1-4}^-$ are shown in Table S2. Due to the high spin multiplicity of $Fe_5S_{1-4}^-$, the spin densities are mainly located on the five iron atoms. It can be seen that the spin densities of the adsorption site decreases significantly after the N_2 adsorption and a redistribution of spin densities among Fe_5 unit appears.

The oxidation state is defined as “the degree of oxidation of an atom in terms of counting electrons”, where the nominal counting of electrons is performed following an agreed set of rules.¹⁰ Electron occupancy gained from NBO analysis can reveal the counting electrons in valence orbitals. The analysis on electron occupancy of each atom in reactant clusters has been performed and the results are given in Table S2. $\Delta(e)$ is the electron occupancy change of each atom in $Fe_5S_{1-4}^-$ compared with the corresponding isolated atom. The electron occupancy in valence orbital of Fe element is $4s^23d^6$. Thus, for Fe1 atom in $Fe_5S_2^-$, $\Delta(e) = 2 + 6 - 0.76 - 6.95 = 0.29$, which indicates that Fe1 donates 0.29 e in the formation of $Fe_5S_2^-$ and the oxidation state of Fe1 is about +0.3. Similarly, the oxidation state of each iron center is in the range of $-0.1 \sim +0.4$ in Fe_5S^- , $+0.2 \sim 0.4$ in $Fe_5S_2^-$, $+0.4 \sim 0.6$ in $Fe_5S_3^-$ and $+0.5 \sim 0.7$ in $Fe_5S_4^-$. Thus, the average oxidation state of each Fe atom in $Fe_5S_{1-4}^-$ can be considered as +0.1 in Fe_5S^- , +0.3 in $Fe_5S_2^-$, +0.4 in $Fe_5S_3^-$ and +0.6 in $Fe_5S_4^-$. Obviously, with the increasing number of S atoms, the degree of oxidation of iron centers gradually increases.

6. References

- (1) Yuan, Z.; Zhao, Y. X.; Li, X. N.; He, S. G. Reactions of $V_4O_{10}^+$ Cluster Ions with Simple Inorganic and Organic Molecules. *Int. J. Mass spectrom.* **2013**, 354-355, 105-112.
- (2) Wu, X. N.; Xu, B.; Meng, J. H.; He, S. G. C–H Bond Activation by Nanosized Scandium Oxide Clusters in Gas-phase. *Int. J. Mass spectrom.* **2012**, 310, 57-64.
- (3) Frisch, M. J. T. G. W.; Schlegel, H. B.; Scuseria, G. E.; Robb, M. A.; Cheeseman, J. R.; Scalmani, G.; Barone, V.; Mennucci, B.; Petersson, G. A.; Nakatsuji, H., et al. Gaussian 09, Revision A.1, Gaussian, Inc. Wallingford CT, 2009.
- (4) Ding, X. L.; Li, Z. Y.; Meng, J. H.; Zhao, Y. X.; He, S. G. Density-functional Global Optimization of $(La_2O_3)_n$ clusters. *J. Chem. Phys.* **2012**, 137, 214311-7.
- (5) Frisch, M. J.; Pople, J. A.; Binkley, J. S. Self-Consistent Molecular Orbital Methods 25. Supplementary Functions for Gaussian Basis Sets. *J. Chem. Phys.* **1984**, 80, 3265-3269.
- (6) Zhao, Y.; Truhlar, D. G. A New Local Density Functional for Main-group Thermochemistry, Transition Metal Bonding, Thermochemical Kinetics, and Noncovalent Interactions. *J. Chem. Phys.* **2006**, 125, 194101-18.
- (7) Yin, S.; Bernstein, E. R. Photoelectron Spectroscopy and Density Functional Theory Studies of Iron Sulfur $(FeS)_m^-$ ($m = 2-8$) Cluster Anions: Coexisting Multiple Spin States. *J. Phys. Chem. A* **2017**, 121, 7362-7373.
- (8) Glendening, E. D.; Badenhoop, J. K.; Reed, A. E.; Carpenter, J. E.; Bohmann, J. A.; Morales, C. M.; Landis, C. R.; Weinhold, F. Theoretical Chemistry Institute, University of Wisconsin, Madison, WI. 2013. <http://nbo6.chem.wisc.edu/>.
- (9) Lu, T.; Chen, F. Multiwfn: A Multifunctional Wavefunction Analyzer. *J. Comput. Chem.* **2012**, 33, 580-592.
- (10) *IUPAC Compendium of Chemical Terminology* 2nd edn (eds McNaught, A. D. & Wilkinson, A.) (Blackwell Scientific, Oxford, **1997**); <https://doi.org/10.1351/goldbook.O04365>